Journal of Applied Polymer Science

Effect of tungsten disulfide nanotubes on the thermomechanical properties of polypropylene-*graft*-maleic anhydride nanocomposites

Apostolos Baklavaridis,[1,2] Ioannis Tsiaoussis,[3] Costas Panayiotou,[2] Ioannis Zuburtikudis[1,4]

[1]Department of Mechanical and Industrial Design Engineering, TEI of Western Macedonia, Kozani 50100, Greece
[2]Department of Chemical Engineering, Aristotle University of Thessaloniki, Thessaloniki 54124, Greece
[3]Department of Physics, Aristotle University of Thessaloniki, Thessaloniki 54124, Greece
[4]Currently on a Leave of Absence and with the Department of Chemical and Petroleum Engineering, United Arab Emirates University, Al Ain, U.A.E
Correspondence to: I. Zuburtikudis (E-mail: ioannis.z@uaeu.ac.ae or izub@teikoz.gr)

ABSTRACT: In this work, the influence of tungsten disulfide nanotubes (INT-WS_2) on the mechanical, thermal, structural, and morphological characteristics of Polypropylene-graft-maleic anhydride (PPGMA) nanocomposites is investigated. The addition of 5% INT-WS_2 increases the Young's Modulus by 28.5% and the storage modulus by 196.5% (in the rubbery state). Furthermore, the nanocomposites' thermal stability increases (up to 10 °C) with the addition of INT-WS_2. Transmission electron microscopy observations of the nanocomposites revealed that nanotubes' length is significantly reduced during processing and that nanotubes are well-dispersed inside the PPGMA matrix. DSC results indicated that INT-WS_2 serve as nucleating agents in PPGMA. Moreover, AFM observations (coupled with DSC results) suggested the formation of fibrillar crystallites in the nanocomposites. This interfacial crystalline structure seems to interpose between the PPGMA and INT-WS_2. Thus, it plays a crucial role in the load transfer from the amorphous part of the polymer to the rather stiff INT-WS_2. © 2016 Wiley Periodicals, Inc. J. Appl. Polym. Sci. **2016**, *133*, 43887.

KEYWORDS: composites; functionalization of polymers; graphene and fullerenes; mechanical properties; nanotubes; thermal properties

Received 8 December 2015; accepted 29 April 2016
DOI: 10.1002/app.43887

INTRODUCTION

Polypropylene (PP) is a thermoplastic commodity polymer of great importance because of its low cost, low weight, high thermal stability, resistance to corrosion, moldability, and recyclability. Hence, PP is used extensively in various industrial applications, such as in the automotive, packaging, biomedical, and other industries.[1–5] However, there is a major disadvantage which hinders, to some extent, the use of PP in the aforementioned applications. Even though the crack initiation resistance is quite high, the crack propagation resistance of PP is rather limited.[5] Consequently, when a crack is formed, the breakage can easily occur.

In order to improve the mechanical and other physical properties of PP, significant research efforts aim at developing nano-reinforced PP. Silicate clays[2,6,7] and carbon nanotubes[5,8,9] were extensively investigated as reinforcing elements of PP, while several other nano-fillers are currently being tested.[3,10–12] Layered nanostructures composed of transition metal dichalcogenides consist a promising class of reinforcing nano-fillers. The discovery of tungsten disulfide nanotubes (INT-WS_2), back in 1992, opened the doors to an entire new research field in nanomaterials.[13] INT-WS_2 exhibit some mixed covalent-ionic nature, while their layered-tubular structure resembles the one of multiwall carbon nanotubes (MWNTs). INT-WS_2 combines a variety of interesting characteristics: good mechanical properties (high modulus and compressive strength), low friction coefficient, closed structure, chemical inertness and biocompatibility.[13–20]

The effective dispersion of the nano-fillers inside the polymer matrix is very important in order to achieve the maximum enhancement of the final nanocomposite's properties. However, PP exhibits low polarity and relatively low compatibility with inorganic nano-fillers. The grafting of maleic anhydride onto PP chains is one of the most common methods in order to increase the polarity of polypropylene's chains and consequently the dispersion of nano-fillers inside the PP matrix.[21–23]

Polypropylene-graft-maleic anhydride (PPGMA) can play two different roles in the production of PP nanocomposites. Firstly, it can be utilized as compatibilizer in order to increase the interfacial adhesion between PP and the inorganic nano-filler; several studies investigated the effect of PPGMA on the structure, the mechanical and thermal properties of PP nanocomposites.[5,7,21–27]

Secondly, PPGMA can be used itself as the polymer matrix for the production of PPGMA nanocomposites. However, the preservation of the maleic anhydride concentration in relatively low levels (around 0.6%) was found to be vital in order to obtain PPGMA nanocomposites with satisfactory mechanical properties.[7] This is because of the fact that the grafting procedure of maleic anhydride onto polypropylene's chains decreases the molecular weight and usually deteriorates, to some extent, the mechanical properties of PPGMA.[24,28–30] Gilman *et al.* reported the preparation and characterization of clay-reinforced PPGMA nanocomposites with enhanced flammability properties.[31] Tidjani *et al.* investigated the structure, the degradation, and fire behavior of PPGMA loaded with different types of organically modified clays. Their findings suggested that the fine dispersion of the clay sheets inside the PPGMA matrix affects the final properties of the nanocomposites.[32,33]

The mechanical properties of PPGMA nanocomposites have not been thoroughly examined in most of the aforementioned works. Moreover, studies dealing with the preparation and the characterization of PPGMA nanocomposites embedding other types of nano-fillers (e.g. inorganic nanotubes) are still missing. In this work, we report, for the first time, the preparation and the characterization of mechanically strong PPGMA nanocomposites reinforced with INT-WS_2. The addition of 5% INT-WS_2 increases the Young's Modulus by 28.5% and the storage modulus in the rubbery state by 196.5%. Additionally, the thermal degradation behavior of the nanocomposites was improved. The cause of the improvement in the nanocomposite properties lies to the nanostructured morphology and to the good dispersion of the nanotubes inside the PPGMA matrix.

EXPERIMENTAL

Materials

PPGMA containing 0.6 wt % maleic anhydride (Code: 426512) was purchased from Aldrich Chemicals (Germany). INT-WS_2 were purchased from Nanomaterials (Israel). All materials were used as received, without any further treatment.

Preparation of the Nanocomposites

Prior to the preparation of the nanocomposites, all constituents were dried in a vacuum oven overnight at 80 °C so as to remove any absorbed moisture and, then, they were placed in a desiccator. A co-rotating twin-screw micro-extruder/compounder (Haake MiniLab) was used for the production of PPGMA/INT-WS_2 nanocomposites. The temperature was kept constant at 180 °C inside the isothermal barrel. Constant nitrogen flow during mixing prevented thermal degradation of the materials. Homogeneous mixing, at a screw speed of 100 rpm, was achieved by allowing enough time to the mixing process, for the stabilization of the screw torque and the melt's viscosity. Three series of PPGMA nanocomposites with 1%, 3%, and 5% INT-WS_2 were fabricated. Subsequently, the extruded materials were compressed-molded using a hydraulic hot-press in rectangular beams (length × width × thickness = 30 × 10 × 1 mm^3) for the DMTA, in dog-bone shaped bars (according to ASTM D1708) for the tensile test and quadrangular films (30 × 30 × 1 mm^3) for the X-ray Diffraction (XRD) measurements.

Characterization Techniques

The tensile properties of the nanocomposites were investigated using an Instron 3345 universal mechanical testing machine according to ASTM D1708 method at a crosshead speed of 25 mm/min. At least five samples of each concentration were tested and the results were statistically processed in order to obtain the mean and the standard deviation values.

The fracture surfaces of the tensile specimens were examined using Scanning Electron Microscopy (SEM). The images presented in this study were recorded using a JEOL 6610LV scanning electron microscope. Before the SEM observation, the samples were coated with gold using a Quorum 150R S magnetron sputtering device to eliminate charging under the electron beam.

The dynamic mechanical properties were investigated applying Dynamic Mechanical Thermal Analysis. A PL MK-II device, having a dual cantilever geometry head for the specimen clamping, was used for the DMTA measurements. The temperature during the measurement varied from −20 °C (using liquid nitrogen) to 100 °C with 2 °C/min heating rate. The frequency was kept constant at 1Hz during the temperature scan. The storage (E') and loss (E'') moduli versus temperature were recorded and the loss tangent (tanδ) was calculated by dividing the loss modulus with the storage modulus.

The effect of INT-WS_2 on the crystalline structure of PPGMA nanocomposites was studied by means of X-ray Diffraction (XRD), using a 3003 TT Rich. Seifert Diffractometer (Ni filtered Cu Ka radiation, λ_{CuKa} =1.54 Å). The 2θ range scanned was from 5° to 25°.

The melting behavior of the produced nanocomposites was studied by means of Differential Scanning Calorimetry (DSC) using a Bahr 302 DSC device. All DSC scans were carried out under inert (N_2) atmosphere and at a heating rate of 20 °C/min. Each sample was heated initially from 30 °C to 200 °C and then retained in the molten state for 2 min in order to eliminate the thermal history of the sample. The sample was subsequently cooled to 30 °C, at 20 °C/min cooling rate, and then heated again to 200 °C. The endothermic melting peaks were recorded during the second heating procedure. The crystallinity X_c of the PPGMA matrix was determined using the following equation:

$$X_c = \frac{\Delta H_m}{(1-\chi)\times\Delta H_f^o}\times 100 \quad (1)$$

where ΔH_m (J/g) is the enthalpy of melting of the polymer (calculated from the area under the endothermic melting peak), χ is the weight fraction of INT-WS_2 in the nanocomposite, and ΔH_f^o is the enthalpy of fusion of the entirely crystalline PP, taken as 177 J/g according to the literature.[34]

The degradation behavior of the nanocomposites was studied via thermogravimetric analysis (TGA) using a Q500 (TA Instruments) device. The TGA measurements were conducted under pure nitrogen environment at a 20 °C/min heating rate.

The dispersion of INT-WS_2 inside the PPGMA matrix was examined via Transmission Electron Microscopy (TEM) using a JEOL JEM 1010 instrument operated at 100 kV. The samples used for the TEM examination were prepared using a Leica UC7

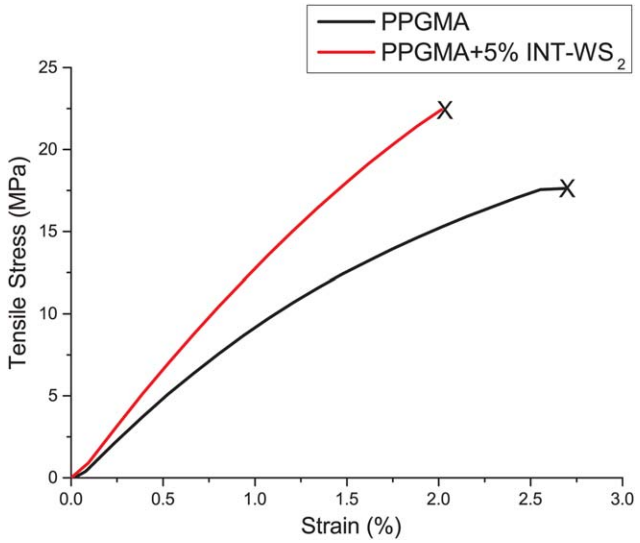

Figure 1. Stress–strain curves of pure PPGMA and the 5% INT-WS_2 loaded nanocomposite at a crosshead speed of 25 mm/min. The X designates the break point. [Color figure can be viewed in the online issue, which is available at wileyonlinelibrary.com.]

ultramicrotome. Ultra-thin segments with nominal thickness 70 nm were cut in room temperature. Subsequently, the segments were deposited on copper grids and were taken for observation.

Atomic Force Microscopy (AFM) was employed in order to examine the surface characteristics of the produced nanocomposites. A Veeco CP-II Scanning Probe Microscope operated in AFM tapping mode was used. The images were recorded at a scan rate of 1 Hz, at room temperature and ambient atmosphere. A commercial silicon tip-cantilever, having a resonance frequency around 300 Hz with a spring constant of 40 N/m and a tip radius of curvature of less than 10 nm, was used. Prior to AFM observation, all samples were heated up to 200 °C (using a heating plate) without covering the surface destined for observation. Subsequently, the samples were cooled down slowly in air (under ambient conditions) in order to exclude the possibility that any nucleating surface altered the crystallite surface morphology of the sample.[35]

RESULTS AND DISCUSSION

Tensile Properties

Characteristic stress–strain curves for pristine PPGMA and the nanocomposite material loaded with 5% INT-WS_2 are presented in Figure 1. PPGMA is a hard and relatively brittle material, since the tensile stress increases linearly with strain until fracture finally occurs. The overall shape of the stress–strain curve of the nanocomposite does not change significantly compared to the one of pristine PPGMA. However, the stress–strain curve of the nanocomposite material loaded with 5% INT-WS_2 exhibits higher slope than the curve of pristine PPGMA. This is attributed to a sharp increase in the Young's Modulus.

The PPGMA/INT-WS_2 nanocomposites' tensile properties are tabulated in Table I. The INT-WS_2 incorporation increases the strength at break up to 20.7% (for the 5% loaded nanocomposite). However, in the lower INT-WS_2 loadings, the recorded tensile strength values are rather similar to those of the pure PPGMA. The INT-WS_2 addition may either inhibit or delay the crack propagation in the nanocomposites. Nevertheless, small amounts of nanotubes do not obstruct the crack spread and the failure inception in the brittle PPGMA matrix. This, will be discussed later, taking into account the SEM morphological observations. This tensile strength fluctuation is rather similar to various nanocomposite systems incorporating carbon nanotubes (CNTs).[5,36] The elongation at break is reduced with the addition of INT-WS_2. Specifically, the elongation at break reduces up to 10.8% for the 5% loaded nanocomposite. Several studies demonstrated the negative nanotubes' impact on the elongation at break of the nanocomposites.[5,37,38] However, the decrease in the elongation at break of the nanocomposites, which is recorded here, is rather small compared to CNT nanocomposites. In addition, the nanocomposites' yield strength increases. Thus, in order to achieve plastic deformation in the nanocomposites, higher stresses are required. Despite the fact that the ASTM 1708 test method is not suggested for the Young's modulus determination, an indication regarding the influence of INT-WS_2 on the stiffness of the nanocomposites can be obtained. As it can be observed from Table I, the addition of INT-WS_2 improves substantially the Young's modulus of the nanocomposites. Thus, a 28.5% increase can be achieved by adding 5% INT-WS_2. Useful connotations, regarding the mechanical behavior of the nanocomposites under tensile loading, can be drawn by correlating the mechanical properties with the crystallinity and the morphological observations. These are all discussed after the presentation of the results regarding the morphology and the crystallinity of the produced nanocomposite materials.

Dynamic Mechanical Properties

In order to gain further insights into the mechanical properties of the nanocomposites, Dynamic Mechanical Thermal Analysis (DMTA) was used. Tan δ as a function of temperature and storage modulus (E') versus temperature are illustrated in Figures 2 and,[3] respectively. The observed peaks in Figure 2 and the step

Table I. Mechanical Characteristics of the Prepared Nanocomposites

Sample	Yield strength (elastic limit) (MPa)	Strength at break (MPa)	Elongation at break (%)	Young's modulus (GPa)
PPGMA	15.23 ± 1.01	20.67 ± 2.26	2.67 ± 0.25	1.05 ± 0.04
PPGMA+1% INT-WS_2	15.11 ± 1.06	20.88 ± 1.15	2.63 ± 0.30	1.01 ± 0.02
PPGMA+3% INT-WS_2	15.96 ± 1.10	21.30 ± 1.55	2.60 ± 0.32	1.07 ± 0.04
PPGMA+5% INT-WS_2	19.10 ± 0.90	24.96 ± 3.58	2.38 ± 0.40	1.35 ± 0.04

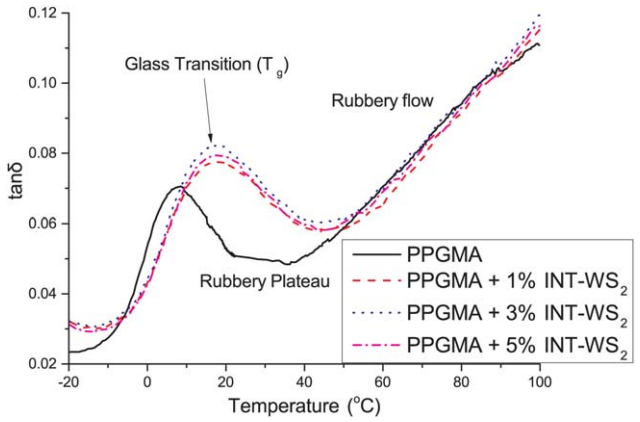

Figure 2. Tan δ vs. temperature curves of the PPGMA/INT-WS_2 nanocomposites. [Color figure can be viewed in the online issue, which is available at wileyonlinelibrary.com.]

change in Figure 3 correspond to the glass transition (T_g) of PPGMA. Rubbery plateau is observed after T_g. Additionally, rubbery flow occurs in higher temperatures. The dynamic mechanical properties of the produced nanocomposites are summarized in Table II. The storage modulus (E') of the nanocomposites increases significantly compared to one of the pristine PPGMA, both in the glassy and the rubbery condition. Specifically, the increase in the storage modulus is rather significant for the materials with high nanotubes' loading (5%), while this increase is not quite notable in low loadings (Table II). The largest improvement (196.5%) in E' is recorded in the rubbery state for the nanocomposite with 5% INT-WS_2. Similar but slightly greater increase in the storage modulus is recorded in isotactic PP nanocomposites reinforced with CNTs.[5,9] Moreover, a remarkable increase in the T_g of the nanocomposites is observed. The T_g of pristine PPGMA is 8.5 °C, while the T_g of the nanocomposites is shifted approximately to 18 °C. In general, the T_g in polymer nanocomposites can be diminished or augmented with the nanofillers' addition.[39] The type of polymer–nanofiller interactions determines the nanocomposites' T_g

Table II. Dynamic Mechanical Properties of the PPGMA/INT-WS_2 Nanocomposites

Sample	E' in the glassy state (−20 °C) (GPa)	E' in the rubbery state (50 °C) (GPa)	Glass transition temperature $-T_g$-(°C)
PPGMA	2.01 ± 0.1	0.58 ± 0.2	8.5
PPGMA+1% INT-WS_2	2.05 ± 0.3	0.80 ± 0.2	17.9
PPGMA+3% INT-WS_2	2.07 ± 0.4	0.98 ± 0.5	18.1
PPGMA+5% INT-WS_2	2.91 ± 0.2	1.72 ± 0.3	17.7

deviation from the T_g value of the pristine polymer. It has been reported that attractive polymer–nanofiller interactions result in augmentations rather than T_g diminutions.[40] The attractive interactions reduce the mobility of the polymer chains surrounding the nanotubes, which means that more energy is needed for the glass to rubber transition. The attractive interactions in our case may be explained by the arrangement of the polymer chains towards the INT-WS_2 and the crystallite and morphological characteristics of the nanocomposites.

Crystalline Structure, Melting and Crystallization Behavior

The XRD patterns of the examined nanocomposite and pure materials are shown in Figure 4. The pattern of pure PPGMA exhibits the characteristic peaks at 2θ = 13.9°, 16.7°, 18.3°, 20.9°, and 21.6° which correspond to the reflections from (110), (040), (130), (111), and (041) planes of the monoclinic crystal type of PP (a-phase). The a-phase of PP is most commonly observed in PP-nanotube nanocomposites.[38,41,42] The absence of the two distinct peaks at 16.2° and 21.2° 2θ, indicates the complete absence of the hexagonal b-phase of PP.[43] In the case of the nanocomposites, the peak positions (Figure 4) corresponding to PPGMA crystal planes remain largely intact and no new

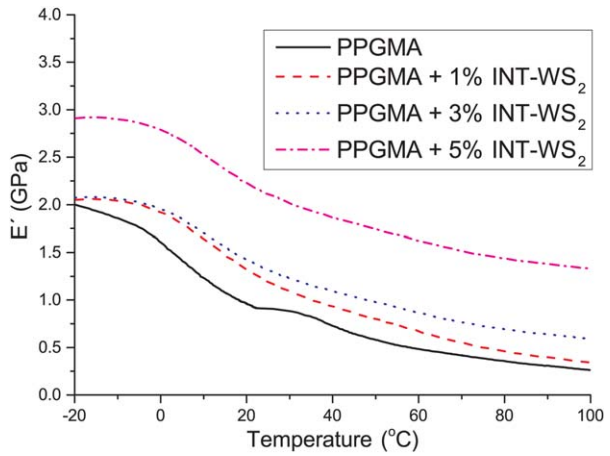

Figure 3. E' vs. temperature curves of the PPGMA/INT-WS_2 nanocomposites. [Color figure can be viewed in the online issue, which is available at wileyonlinelibrary.com.]

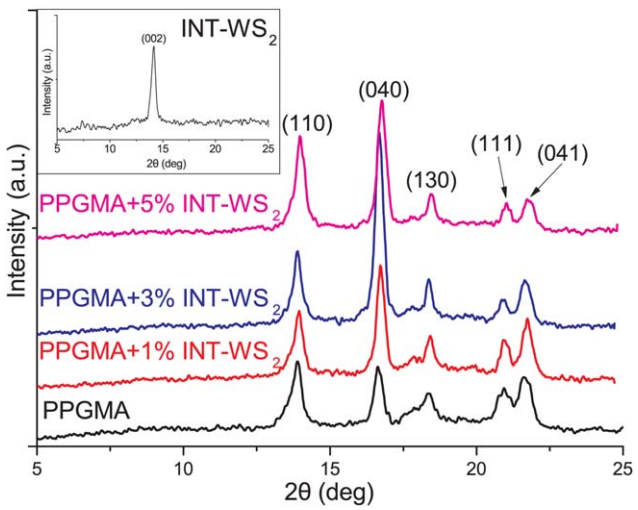

Figure 4. XRD patterns of PPGMA, the PPGMA/INT-WS_2 nanocomposites and pure INT-WS_2. [Color figure can be viewed in the online issue, which is available at wileyonlinelibrary.com.]

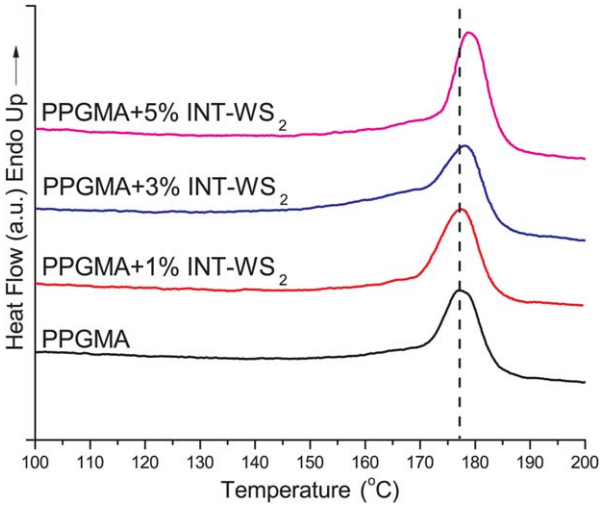

Figure 5. Melting endotherms of PPGMA and the PPGMA/INT-WS_2 nanocomposites. [Color figure can be viewed in the online issue, which is available at wileyonlinelibrary.com.]

peaks arise because of the INT-WS_2 addition. Consequently, the addition of INT-WS_2 does not affect the crystalline type of PPGMA.

The melting and crystallization behavior of the nanocomposites was explored via DSC. In Figure 5 the melting endotherms of the nanocomposites are shown. Furthermore, DSC traces obtained during nonisothermal crystallization are illustrated in Figure 6. Moreover, the crystallization temperature (T_c), the melting point (T_m), the enthalpy of fusion (ΔH_f), and the degree of crystallinity (X_c) of the nanocomposites are summarized in Table III. The incorporation of INT-WS_2 in the PPGMA matrix leads to a T_c (peak value) increase. In higher nanotube loadings this increase is more pronounced. Specifically, T_c increases approximately 8 °C in the nanocomposite with 5% INT-WS_2 loading. Moreover, the T_m (peak value) of pure

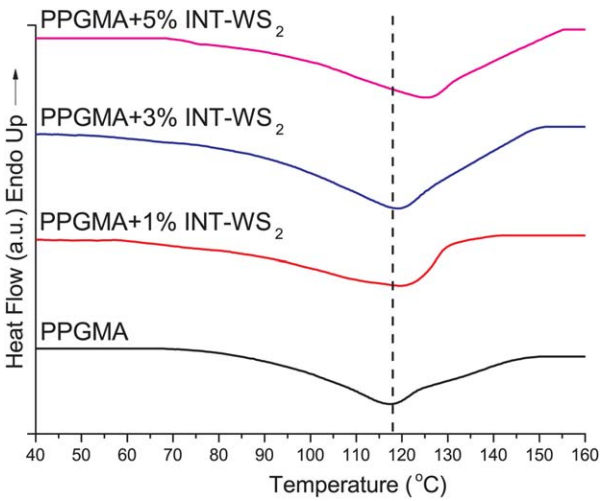

Figure 6. DSC traces of PPGMA and the PPGMA/INT-WS_2 nanocomposites obtained during nonisothermal crystallization at 20 °C/min cooling rate. [Color figure can be viewed in the online issue, which is available at wileyonlinelibrary.com.]

Table III. DSC Results of PPGMA/INT-WS_2 Nanocomposites

Sample	T_c (°C)	T_m (°C)	ΔH_f (J g^{-1})	X_c (%)
PPGMA	117.5	177.1	22.9	13.0
PPGMA+1% INT-WS_2	119.6	177.6	24.0	13.7
PPGMA+3% INT-WS_2	119.3	178.1	23.7	13.8
PPGMA+5% INT-WS_2	125.6	179.1	31.6	18.8

PPGMA is 177.1 °C. By increasing the INT-WS_2 loading in the nanocomposites, T_m is slightly shifted towards higher temperatures. This may be imputed to the creation of narrow sized and more perfectly shaped crystals. Apart from the T_m increase in the nanocomposites, the creation of narrow sized crystals is also supported from the slight change of the shape of the melting endotherm, which is more evident in the nanocomposite with 5% INT-WS_2 loading (Figure 5). Logakis *et al.*[9] suggested that the shape changes in the melting peaks, observed in MWCNT/PP nanocomposites, can be ascribed to one-dimensional growth of PP crystallites in a parallel to the surface direction (transcrystallinity). This type of one-dimensional PP-crystallization procedure is initiated from the nanotubes surface. Moreover, Assouline *et al.*[44] also observed fibrillar crystalline morphologies (palisades) rather than spherulites in MWCNT/PP nanocomposites. Both ΔH_f and X_c increase by adding INT-WS_2 in the nanocomposites. The crystallinity increase is more evident in higher INT-WS_2 loadings (5%). The observed increase in X_c is rather similar to the X_c increase recorded in CNT reinforced PP/PPGMA mixtures.[45] Both the increase in T_c and X_c may be ascribed to the fact that INT-WS_2 promote the heterogeneous nucleation and act as nucleating agents in the INT-WS_2 nanocomposites. Several studies demonstrate the nucleating ability and efficiency of WS_2 nanofillers in PP[10] and other thermoplastic matrices.[46]

Morphological Characterization

Several microscopic techniques were used in order to examine the morphological characteristics of the produced materials. In Figure 7, SEM (a) and TEM (b) images of pristine INT-WS_2 are shown. INT-WS_2 exhibit tubular and multiwall structure, resembling the one of multiwall carbon nanotubes (MWCNTs). The length of INT-WS_2 can reach several microns, while their width ranges within few nanometers.[18,47,48] This is evidenced very clearly by the TEM image of Figure 7. This image shows that the lengths of the particular INT-WS_2 are 4.8, 2, and 1.2 μm, while their width is 0.1 μm (100 nm). In addition, the SAED pattern (solid circles) proves the INT-WS_2 are polycrystalline, in accordance with previous observations.[18]

It is widely accepted that the dispersion of nanosized fillers plays an important role in the enhancement of the mechanical and thermal properties of the nanocomposite systems. In Figure 8 TEM pictures of the 5% INT-WS_2 loaded nanocomposite are shown. Generally, INT-WS_2 appears to be well dispersed in the PPGMA matrix. In Figure 8(a) an alignment of INT-WS_2 is observed. This alignment of INT-WS_2 should be attributed to the shear stresses which are applied to the polymer melt during

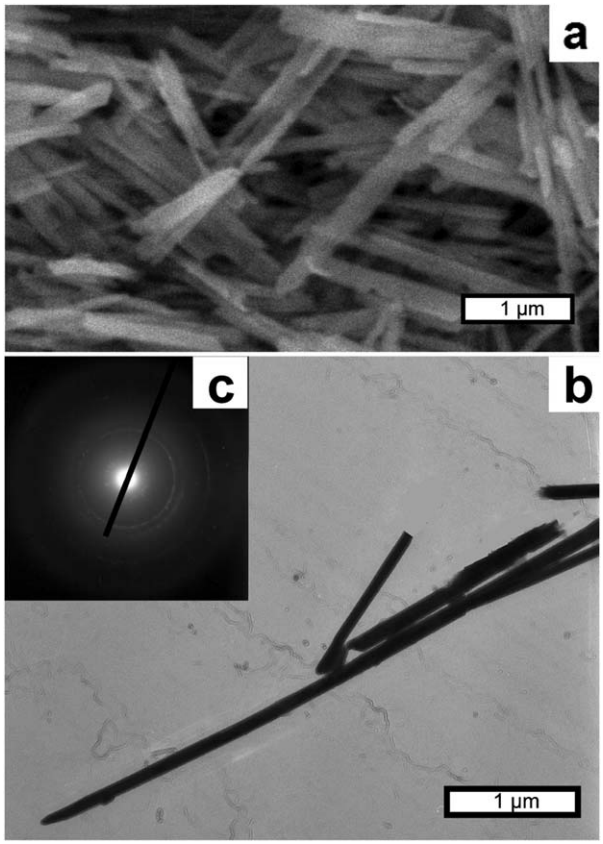

Figure 7. SEM (a) TEM (b) and selected area electron diffraction (SAED) pattern of INT-WS_2.

the extrusion process. Several studies demonstrated the alignment of CNTs during the melt extrusion procedure.[49,50] In Figure 8(b), a rather small aggregation of INT-WS_2 is shown. The as-received INT-WS_2, in the form of dry powder, is aggregated (because of van der Waals forces) into large bundles (with diameters of hundreds of microns). This is attributed to the significant INT-WS_2 length, which can reach several microns. After the fabrication of the nanocomposites via extrusion, the length of the INT-WS_2 is significantly reduced. The reason is twofold. Firstly, during the extrusion process the breakage of the nanotubes may occur because of the high shear stresses applied to the melt. Secondly, the strong interfacial polymer-nanotube interactions may cause fragmentation of the nanotubes.[51] Consequently, the fragmentation of the nanotubes contributes to their disentanglement. This disentanglement is essential in order to achieve fine dispersion of the nanotubes inside the polymer matrix. In our case, the dispersed nanotubes inside the PPGMA matrix are at least three or four times shorter compared to the initial (as-received) nanotubes (Figure 7). As shown in Figure 8(a, b) the length of the dispersed INT-WS_2 inside the PPGMA matrix is usually less than 1 μm. In previous studies dealing with isotactic PP-CNT nanocomposites, the improved dispersion of the nanotubes inside the polymer matrix was attributed to their disentanglement and their length reduction.[38] In this study, the dispersion of the INT-WS_2 is further facilitated because of the polar nature of PPGMA.

In order to gain further insights into the surface morphology of the nanocomposites AFM was employed. In Figure 9(a,b) the surface topography of pure PPGMA and the nanocomposite with 5% INT-WS_2 are shown, respectively. The INT-WS_2 addition affects the surface topography of the nanocomposites. An evident surface roughness increase is observed in the nanocomposites. Moreover, in Figure 9(b) a fibrillar surface morphology is observed. This morphology is related to the PP fibrils (approximately 100 nm each) which are arranged in rows of palisades parallel to the surface. Similar fibrillar crystalline structures of PP have been previously observed.[35,52]

The fracture surfaces of the nanocomposites that occurred during tensile testing were examined with SEM. In Figure 10 SEM micrographs of the fracture surfaces of pristine PPGMA (a) and the nanocomposite with 5% INT-WS_2 (b) are presented. The fracture surface of pristine PPGMA is relatively smooth and the cracks are spreading easily throughout the brittle PPGMA matrix. The addition of INT-WS_2 in the nanocomposites causes an increase in the roughness of the fracture surface. When a crack meets nanotubes oriented perpendicularly to the crack spreading direction, it can buckle along the region adjacent to the polymer–nanotube interface. Whilst the nanotube concentration increases, the distance between the individual nanotubes decreases. In that sense the length and the tortuosity of the crack's pathway increases, which leads to an increase in the surface roughness.[53,54] Moreover, the failure of the nanocomposites seems to occur because of microcracks merging. The

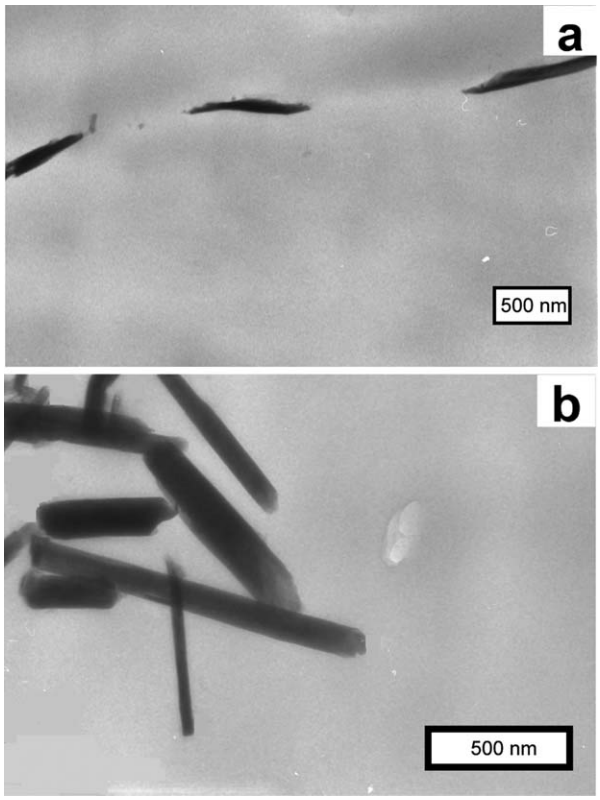

Figure 8. TEM images of the nanocomposite PPGMA + 5% INT-WS_2 nanocomposite: (a) nanotube alignment along the extrusion direction, (b) rather small INT-WS_2 aggregation inside the PPGMA matrix.

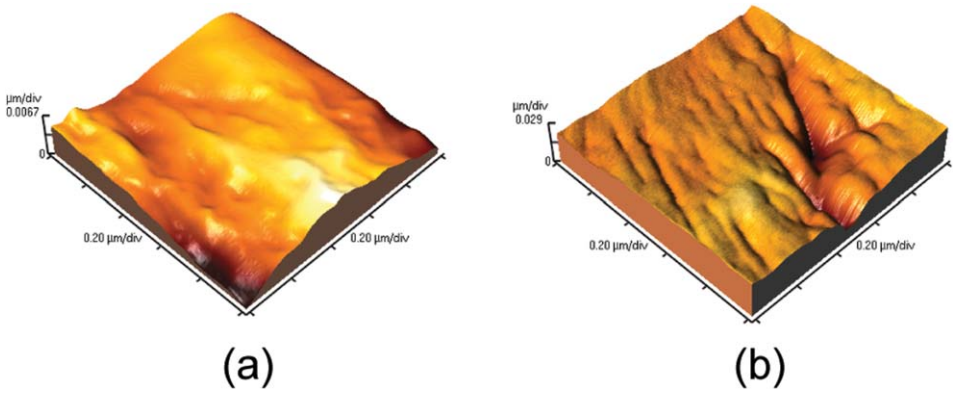

Figure 9. (a) AFM pictures of PPGMA (a) and (b) the PPGMA + 5% INT-WS_2 nanocomposite. [Color figure can be viewed in the online issue, which is available at wileyonlinelibrary.com.]

propagation and merging of microcracks is delayed because of the increase of crack's pathway length and tortuosity. This should also contribute to the observed increase of the tensile strength of the nanocomposites.

Useful insights regarding the reinforcing mechanisms which are responsible for the mechanical properties enhancement can be drawn by coupling the morphological observations of the nanocomposites with the mechanical properties measurements. The nanotubes length plays an important role in the mechanical behavior of the nanocomposites.[55] When the nanotubes are short, the mechanical properties of the nanocomposites depend on the nanotube-polymer interface. On the other hand, the mechanical properties are based on the strength of the nanotubes when the nanotubes are long. The TEM observations (Figures 7 and 8) suggest that the INT-WS_2 are relatively short, well dispersed and oriented inside the PPGMA matrix. In this case, the favorable polymer-nanotube interactions play a more significant role in the enhancement of the mechanical properties. Furthermore, the significant augmentation in the Young's modulus, the yield strength, the strength at break and the storage modulus may be related with the fibrillar crystalline structure of PPGMA, as shown from the AFM images (Figure 9) and the DSC results. Since the crystallinity of PPGMA is relatively low and the nucleation of the PPGMA fibril crystals starts from the surface of the nanotubes, the following conclusion can be drawn: the load should be transferred effectively from the amorphous part of PPGMA to the rather stiff INT-WS_2 because of the crystalline layer, which is formed around the nanotubes. Moreover, the enhancement in the mechanical properties deriving from any crystalline form conversion of PPGMA should be excluded since the XRD measurements provided no such evidence. Similar findings regarding the reinforcing mechanism in CNT-polymer nanocomposites have been reported.[9,56] Even though INT-WS_2 has a positive effect on the majority of the mechanical properties, the elongation at break (Table I) slightly decreases with the addition of INT-WS_2. In most cases reported in the literature, the incorporation of inorganic nanofillers inside the polymer matrix decreases significantly the elongation at break of the nanocomposites and the breakage occurs right after the yield point. This can be attributed to various reasons. Prashantha *et al.*[57] attributed the reduction of the elongation at break to the presence of nanotube aggregates inside the nanocomposites. Micusik *et al.*[45] observed that the nanocomposites with lower concentrations of nanotubes exhibit higher elongation than the nanocomposites with higher nanotube content. They attributed the significant decrease in the elongation at break, with the nanotubes addition, to the decrease of the amorphous part of the polymer (X_c increase). Since in PPGMA/INT-WS_2 nanocomposites the aggregation of the nanotubes is rather insignificant (Figure 8), the decrease in the elongation at break should be attributed to the reduction of the amorphous part of the polymer (increase in X_c). Indeed, the largest decrease in the elongation at break (Table I) is recorded in the nanocomposite (5%) with the highest X_c (Table III).

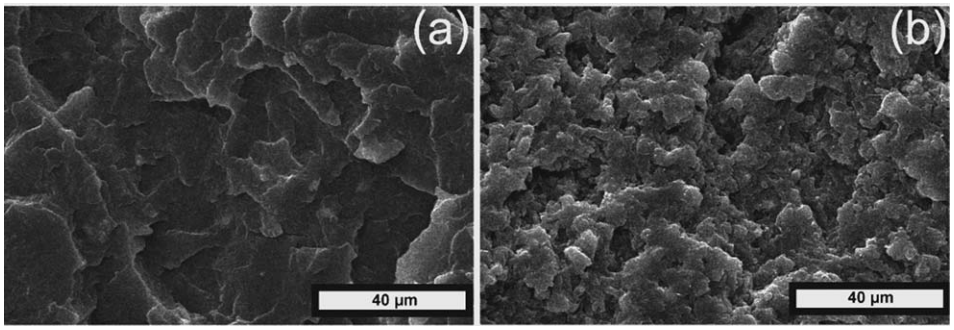

Figure 10. SEM micrographs of (a) the fracture surfaces of PPGMA and (b) the PPGMA + 5% INT-WS_2 nanocomposite. The fracture surfaces occurred during tensile testing.

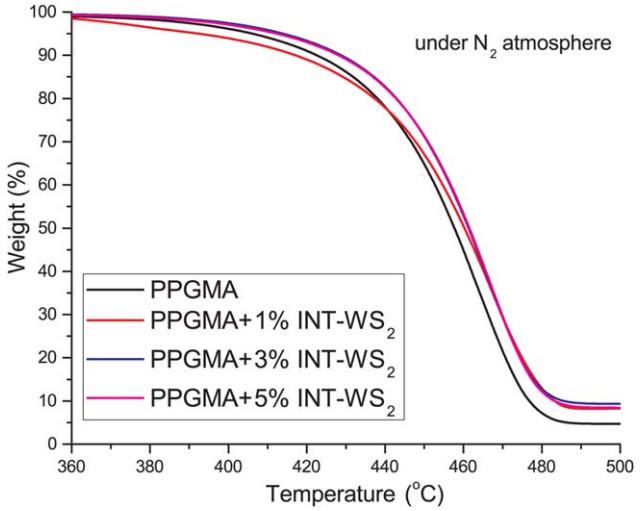

Figure 11. TGA curves of PPGMA and its nanocomposites incorporating INT-WS_2, under N_2 atmosphere. [Color figure can be viewed in the online issue, which is available at wileyonlinelibrary.com.]

Thermal Degradation Behavior

The influence of INT-WS_2 on the degradation behavior of the PPGMA/INT-WS_2 nanocomposites was examined using TGA. The thermogravimetric and the derivative thermogravimetric curves are shown in Figures 11 and 12, respectively. Moreover, all the characteristic temperatures, which describe the thermal degradation of PPGMA and PPGMA/INT-WS_2 nanocomposites are summarized in Table IV. PPGMA and PPGMA/INT-WS_2 nanocomposites decompose through a one-step degradation process (Figure 11). The addition of INT-WS_2 in the PPGMA matrix improves the nanocomposites' thermal stability. The thermal degradation of pure PPGMA is initiated at the temperature of 393.9 °C, while the degradation's initiation temperature ($T_{on(3\%)}$) in the nanocomposites increases up to 10 °C in the 3% INT-WS_2 loaded nanocomposite. This increase is comparable with the one observed in other nanotube reinforced polymer nanocomposites.[38,58] The improved thermal degradation behavior of the INT-WS_2 nanocomposites can be attributed to two main factors. Firstly, the improved degradation behavior of the nanocomposites can be ascribed to the inability of the degradation products to diffuse through the material to the gaseous phase, because of the entanglements formed between the polymer chains and the INT-WS_2.[59,60] Secondly, the improvement can be attributed to the increase of the activation energy of the degradation process caused by the favorable (attractive) interactions between PPGMA and INT-WS_2.[58] Even though the addition of INT-WS_2 generally improves the thermal stability of the nanocomposites, it is worth noting that the degradation initiation temperature ($T_{on(3\%)}$) for the 1% INT-WS_2 loaded nanocomposite is lower than the one observed for pure PPGMA. Similar behavior has been observed in PP/CNT nanocomposites, and it may be attributed to some remaining inorganic elements deriving from the catalyst which was used during the preparation of the nanotubes.[38]

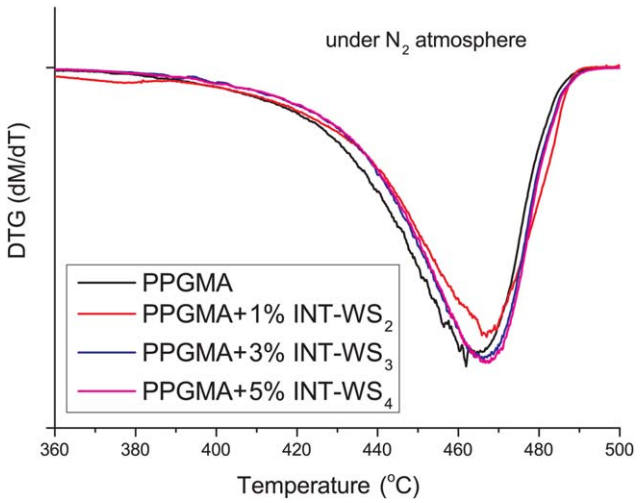

Figure 12. Derivative mass loss (DTG) vs temperature curves of PPGMA and its nanocomposites incorporating INT-WS_2, under inert atmosphere. [Color figure can be viewed in the online issue, which is available at wileyonlinelibrary.com.]

Table IV. TGA Data of PPGMA and its Nanocomposites with INT-WS_2

Sample	$T_{on(3\%)}$[a] (°C)	$T_{d(20\%)}$[b] (°C)	$T_{d(max)}$[c] (°C)	T_{END}[d] (°C)
PPGMA	393.9	437.9	461.9	482.7
PPGMA+1% INT-WS_2	375.3	437.3	467.1	490.0
PPGMA+3% INT-WS_2	403.3	442.8	467.7	484.0
PPGMA+5% INT-WS_2	400.7	442.8	467.9	484.6

[a] $T_{on(3\%)}$ is the degradation's onset temperature at 3% mass loss.
[b] $T_{d(20\%)}$ is the degradation temperature at 20% mass loss.
[c] $T_{d(max)}$ is the maximum degradation rate temperature obtained at the minimum point of the DTG curve (peak).
[d] T_{END} is the offset degradation temperature.

CONCLUSIONS

PPGMA nanocomposites containing INT-WS_2 were successfully produced using the melt mixing technique. The INT-WS_2 addition augmented both the tensile and dynamic mechanical properties of the PPGMA nanocomposites. Specifically, the addition of 5% INT-WS_2 increases the Young's Modulus by 28.5% and the storage modulus in the rubbery state by 196.5%. TEM observations have shown that the length of the nanotubes is significantly reduced during processing. Moreover, relatively good dispersion and orientation of INT-WS_2 inside the PPGMA matrix was observed via TEM examination. Both the dispersion and orientation of INT-WS_2 have partly affected the mechanical properties enhancement. DSC results indicated that INT-WS_2 act as nucleating agents in PPGMA. Moreover, the melting peak shape change with the addition of INT-WS_2, coupled with AFM observations suggested the formation of fibrillar crystallites, arranged in rows of palisades parallel to the surface of the nanocomposites. This interfacial crystalline structure seems to interpose between the PPGMA and INT-WS_2, playing a crucial role in the load transfer from the amorphous part of the polymer to the rather stiff INT-WS_2. Finally, the TGA results denoted a thermal stability increase (up to 10 °C) with the addition of INT-WS_2.

ACKNOWLEDGMENTS

The authors would like to thank the COINAPO (Composites of Inorganic Nanotubes and Polymers) COST Action MP0902 for providing a conducive environment for stimulating discussions during the workshops and summer schools.

REFERENCES

1. Moore, E. P. Polypropylene Handbook: Polymerization, Characterization, Properties, Processing, Applications; Hanser Publishers: New York, **1996**.
2. Jang, L. W.; Kim, E. S.; Kim, H. S.; Yoon, J. S. *J. Appl. Polym. Sci.* **2005**, *98*, 1229.
3. Chan, K. W.; Wong, H. M.; Yeung, K. W. K.; Tjong, S. C. *Materials* **2015**, *8*, 992.
4. Gorgieva, S.; Modic, M.; Dovgan, B.; Kaisersberger-Vincek, M.; Kokol, V. *Plasma Process. Polym.* **2015**, *12*, 237.
5. Bikiaris, D. *Materials* **2010**, *3*, 2884.
6. Chrissopoulou, K.; Altintzi, I.; Andrianaki, I.; Shemesh, R.; Retsos, H.; Giannelis, E. P.; Anastasiadis, S. H. *J. Polym. Sci. Part B: Polym. Phys.* **2008**, *46*, 2683.
7. Svoboda, P.; Zeng, C.; Wang, H.; Lee, L. J.; Tomasko, D. L. *J. Appl. Polym. Sci.* **2002**, *85*, 1562.
8. Verma, P.; Saini, P.; Malik, R. S.; Choudhary, V. *Carbon* **2015**, *89*, 308.
9. Logakis, E.; Pollatos, E.; Pandis, C.; Peoglos, V.; Zuburtikudis, I.; Delides, C. G.; Vatalis, A.; Gjoka, M.; Syskakis, E.; Viras, K.; Pissis, P. *Compos. Sci. Technol.* **2010**, *70*, 328.
10. Naffakh, M.; Martin, Z.; Fanegas, N.; Marco, C.; Gomez, M. A.; Jimenez, I. *J. Polym. Sci., Part B: Polym. Phys.* **2007**, *45*, 2309.
11. Herrera-Ramírez, L. C.; Castell, P.; Fernández-Blázquez, J. P.; Fernández, T.; Guzmán de Villoria, R. *Compos. Sci. Technol.* **2015**, *111*, 9.
12. Bari, P.; Lanjewar, S.; Hansora, D. P.; Mishra, S. *J. Appl. Polym. Sci.* **2016**, *133*, DOI: 10.1002/app.42927.
13. Tenne, R.; Margulis, L.; Genut, M.; Hodes, G. *Nature* **1992**, *360*, 444.
14. Zak, A.; S.-E, L.; Efrati, R.; Drangai, L.; Fleischer, N.; Tenne, R. *Sens. Transducers J.* **2011**, *12*, 1.
15. Naffakh, M.; Marco, C.; Gomez, M. A.; Jimenez, I. *Mater. Chem. Phys.* **2011**, *129*, 641.
16. Andre, B.; Gustavsson, F.; Svahn, F.; Jacobson, S. *Surf. Coat. Technol.* **2012**, *206*, 2325.
17. Kaplan-Ashiri, I.; Cohen, S. R.; Gartsman, K.; Rosentsveig, R.; Seifert, G.; Tenne, R. *J. Mater. Res.* **2004**, *19*, 454.
18. Rothschild, A.; Sloan, J.; Tenne, R. *J. Am. Chem. Soc.* **2000**, *122*, 5169.
19. Lalwani, G.; Henslee, A. M.; Farshid, B.; Parmar, P.; Lin, L.; Qin, Y. X.; Kasper, F. K.; Mikos, A. G.; Sitharaman, B. *Acta Biomater.* **2013**, *9*, 8365.
20. Goldman, E. B.; Zak, A.; Tenne, R.; Kartvelishvily, E.; Levin-Zaidman, S.; Neumann, Y.; Stiubea-Cohen, R.; Palmon, A.; Hovav, A. H.; Aframian, D. J. *Tissue Eng. Part A* **2015**, *21*, 1013.
21. Chiu, F. C.; Lai, S. M.; Chen, J. W.; Chu, P. H. *J. Polym. Sci. Part B: Polym. Phys.* **2004**, *42*, 4139.
22. García-López, D.; Picazo, O.; Merino, J. C.; Pastor, J. M. *Eur. Polym. J.* **2003**, *39*, 945.
23. Kawasumi, M.; Hasegawa, N.; Kato, M.; Usuki, A.; Okada, A. *Macromolecules* **1997**, *30*, 6333.
24. Ding, C.; He, H.; Guo, B. C.; Jia, D. M. *Polym. Compos.* **2008**, *29*, 698.
25. Chen, X.; Hu, J.; Zhou, L.; Li, W.; Yang, Z.; Wang, Y. *J. Mater. Sci. Technol.* **2008**, *24*, 279.
26. Lee, S. H.; Cho, E.; Jeon, S. H.; Youn, J. R. *Carbon* **2007**, *45*, 2810.
27. Pedrazzoli, D.; Pegoretti, A.; Kalaitzidou, K. *Polym. Compos.* **2015**, DOI: 10.1002/pc.23380.
28. Hasegawa, N.; Okamoto, H.; Kato, M.; Usuki, A. *J. Appl. Polym. Sci.* **2000**, *78*, 1918.
29. Wang, Y.; Chen, F. B.; Li, Y. C.; Wu, K. C. *Compos. Part B* **2004**, *35*, 111.
30. Reichert, P.; Nitz, H.; Klinke, S.; Brandsch, R.; Thomann, R.; Mülhaupt, R. *Macromol. Mater. Eng.* **2000**, *275*, 8.
31. Gilman, J. W.; Jackson, C. L.; Morgan, A. B.; Harris, R.; Manias, E.; Giannelis, E. P.; Wuthenow, M.; Hilton, D.; Phillips, S. H. *Chem. Mater.* **2000**, *12*, 1866.
32. Tidjani, A. *Polym. Degrad. Stab.* **2005**, *87*, 43.
33. Tidjani, A.; Wald, O.; Pohl, M. M.; Hentschel, M. P.; Schartel, B. *Polym. Degrad. Stab.* **2003**, *82*, 133.
34. Li, J. X.; Cheung, W. L.; Jia, D. *Polymer* **1999**, *40*, 1219.
35. van Krevelen, D. W.; te Nijenhuis, K. Properties of Polymers: Their Correlation with Chemical Structure; their Numerical Estimation and Prediction from Additive Group Contributions; Elsevier: Amsterdam, **2009**.
36. Yang, W.; Zhou, H.; Yang, B.; Lu, H.; Song, L.; Hu, Y. *Polym. Compos.* **2015**, DOI: 10.1002/pc.23354.
37. Grigoriadou, I.; Paraskevopoulos, K. M.; Karavasili, M.; Karagiannis, G.; Vasileiou, A.; Bikiaris, D. *Compos. Part B* **2013**, *55*, 407.
38. Bikiaris, D.; Vassiliou, A.; Chrissafis, K.; Paraskevopoulos, K. M.; Jannakoudakis, A.; Docoslis, A. *Polym. Degrad. Stabil.* **2008**, *93*, 952.
39. Rittigstein, P.; Torkelson, J. M. *J. Polym. Sci. Part B: Polym. Phys.* **2006**, *44*, 2935.
40. Keddie, J. L.; Jones, R. A. L.; Cory, R. A. *Faraday Discuss.* **1994**, *98*, 219.
41. Satapathy, B. K.; Ganß, M.; Weidisch, R.; Pötschke, P.; Jehnichen, D.; Keller, T.; Jandt, K. D. *Macromol. Rapid Commun.* **2007**, *28*, 834.
42. Seo, M. K.; Lee, J. R.; Park, S. *J. Mater. Sci. Eng. A* **2005**, *404*, 79.
43. Bhattacharyya, A. R.; Sreekumar, T. V.; Liu, T.; Kumar, S.; Ericson, L. M.; Hauge, R. H.; Smalley, R. E. *Polymer* **2003**, *44*, 2373.
44. Assouline, E.; Lustiger, A.; Barber, A. H.; Cooper, C. A.; Klein, E.; Wachtel, E.; Wagner, H. D. *J. Polym. Sci. Part B: Polym. Phys.* **2003**, *41*, 520.

45. Micusik, M.; Omastova, M.; Krupa, I.; Prokes, J.; Pissis, P.; Logakis, E.; Pandis, C.; Potschke, P.; Pionteck, J. *J. Appl. Polym. Sci.* **2009**, *113*, 2536.
46. Naffakh, M.; Marco, C.; Ellis, G.; Cohen, S. R.; Laikhtman, A.; Rapoport, L.; Zak, A. *Mater. Chem. Phys.* **2014**, *147*, 273.
47. Bar Sadan, M.; Heidelmann, M.; Houben, L.; Tenne, R. *Appl. Phys. A: Mater. Sci. Process.* **2009**, *96*, 343.
48. Zak, A.; Sallacan-Ecker, L.; Margolin, A.; Genut, M.; Tenne, R. *Nano* **2009**, *4*, 91.
49. Ahir, S. V.; Huang, Y. Y.; Terentjev, E. M. *Polymer* **2008**, *49*, 3841.
50. Sulong, A. B.; Park, J. *J. Compos. Mater.* **2011**, *45*, 931.
51. Dresselhaus, M. S.; Smalley, R. E.; Dresselhaus, G.; Avouris, P. Carbon Nanotubes: Synthesis, Structure, Properties, and Applications; Springer: Berlin-Heidelberg, **2001**.
52. Michler, G. H.; Baltá-Calleja, F. J. Mechanical Properties of Polymers based on Nanostructure and Morphology; CRC Press: Boca Raton, Florida, **2005**.
53. Marras, S. I.; Zuburtikudis, I.; Panayiotou, C. *Eur. Polym. J.* **2007**, *43*, 2191.
54. Wang, K.; Chen, L.; Wu, J.; Toh, M. L.; He, C.; Yee, A. F. *Macromolecules* **2005**, *38*, 788.
55. Arash, B.; Wang, Q.; Varadan, V. K. *Sci. Rep.* **2014**, *4*, 6479.
56. Coleman, J. N.; Cadek, M.; Ryan, K. P.; Fonseca, A.; Nagy, J. B.; Blau, W. J.; Ferreira, M. S. *Polymer* **2006**, *47*, 8556.
57. Prashantha, K.; Soulestin, J.; Lacrampe, M. F.; Claes, M.; Dupin, G.; Krawczak, P. *eXPRESS Polym. Lett.* **2008**, *2*, 735.
58. Marosfoi, B. B.; Szabó, A.; Marosi, G.; Tabuani, D.; Camino, G.; Pagliari, S. *J. Therm. Anal. Calorim.* **2006**, *86*, 669.
59. O'Connell, M. J.; Boul, P.; Ericson, L. M.; Huffman, C.; Wang, Y.; Haroz, E.; Kuper, C.; Tour, J.; Ausman, K. D.; Smalley, R. E. *Chem. Phys. Lett.* **2001**, *342*, 265.
60. Yang, J.; Lin, Y.; Wang, J.; Lai, M.; Li, J.; Liu, J.; Tong, X.; Cheng, H. *J. Appl. Polym. Sci.* **2005**, *98*, 1087.